

# Compton reflection and the variable X-ray spectrum of NGC 5548

K. Nandra,<sup>1</sup> K. A. Pounds,<sup>1</sup> G. C. Stewart,<sup>1</sup> I. M. George,<sup>2</sup> K. Hayashida,<sup>3</sup> F. Makino<sup>3</sup> and T. Ohashi<sup>4</sup>

<sup>1</sup>*Department of Physics and Astronomy, University of Leicester, University Road, Leicester LE1 7RH*

<sup>2</sup>*Institute of Astronomy, Madingley Road, Cambridge CB3 0HA*

<sup>3</sup>*Institute of Space and Astronautical Science, 3-1-1, Yoshinodai, Sagami-hara, Kanagawa 229, Japan*

<sup>4</sup>*Department of Physics, The University of Tokyo, 3-1, Hongo 7-chome, Bunkyo-ku, Tokyo 113, Japan*

Accepted 1990 September 27. Received 1990 September 20; in original form 1990 August 6

## SUMMARY

Spectral analysis of *EXOSAT* and *Ginga* observations of the Seyfert galaxy NGC 5548 has revealed a complex spectral form. At least four components, a steep non-thermal power law, an iron line, a ‘hard tail’ and a soft emission component, have been identified in the 0.05–20 keV range. The soft component arises from thermal emission by optically thick material. Hard X-ray illumination of this material gives rise to the hard tail, by continuum Compton reflection, and the bulk of the iron line, via fluorescence. Varying relative levels of the power law and reflected continua result in apparent spectral index variations. Spectral and temporal considerations lead us to the conclusion that the material lies close to the central energy source. We suggest that a region of highly ionized gas also contributes to the observed features, and changes in the ionization state of this material cause both variations in the measured low-energy column density and the relative amplitudes of hard and soft X-ray variability. The fact that the intrinsic power-law index of NGC 5548,  $\Gamma \sim 1.9$ , is steeper than the ‘canonical’ index,  $\Gamma = 1.7$ , has important consequences, both for emission models and spectral modelling of Seyfert type AGN.

## 1 INTRODUCTION

Observational evidence is growing to support the hypothesis that dense ( $\geq 10^{10} \text{ cm}^{-3}$ ), ‘cold’ ( $< 10^6 \text{ K}$ ) matter surrounds the central black hole in Active Galactic Nuclei (AGN). The ‘big blue bump’ in the ultraviolet (UV) band (e.g. Shields 1978), and the ‘soft X-ray excesses’ at energies  $< 2 \text{ keV}$  (e.g. Arnaud *et al.* 1985; Pounds *et al.* 1986) are normally interpreted as the thermal emission from such material. Both have been found to be a common property of AGN (Malkan & Sargent 1982; Wilkes & Elvis 1987; Turner & Pounds 1989). Additional spectral features have been predicted due to the reprocessing of the primary X-rays by such local cold matter – notably iron *K*-shell features and a  $\sim 30\text{-keV}$  ‘Compton reflection hump’ (e.g. Guilbert & Rees 1988; Lightman & White 1988; Fabian *et al.* 1989; George & Fabian 1991). Until recently, evidence for such features in AGN was scarce. Except for the well-studied cases of the brightest Seyfert I galaxy NGC 4151 (Warwick *et al.* 1989, and references therein) and the radio galaxy Cen A (Mushotzky *et al.* 1978; Inoue 1985) detections of low significance had been reported in only a handful of cases (e.g.

NGC 5548, Hayes *et al.* 1980; NGC 5506, MCG-5-23-16, NGC 2992, Mushotzky 1982; Mrk 509, Morini, Lipani & Molteni 1987). However, since the launch of *Ginga* in 1987 it has become clear that *K*-shell features are common in the X-ray spectra of AGN (e.g. Nandra *et al.* 1989; Pounds *et al.* 1989; Nandra, Pounds & Stewart 1990; Pounds *et al.* 1990; Turner *et al.* 1990; Matsuoka *et al.* 1990).

Such observations raise questions as to the location and physical condition of the matter responsible for the reprocessing. The majority of the sources found to exhibit spectral features have low intrinsic line-of-sight column densities; hence the reprocessing is, in general, unlikely to take place within a shell of covering material, as proposed for the heavily obscured sources Cen A and NGC 4151 (Inoue 1985; Warwick *et al.* 1989). The mean energy of the emission line is, in most cases,  $\sim 6.4 \text{ keV}$ , consistent with *K*- $\alpha$  fluorescence from iron in a low state of ionization. Furthermore, in one source, NGC 6814 (Kunieda *et al.* 1990), the line has been seen to respond to variations in the continuum on a very short time-scale ( $< 300 \text{ s}$ ). Whilst, as discussed below, temporal variations are difficult to interpret, it is clear that at least in the case of NGC 6814, the

material responsible for the reprocessing lies very close to the source of primary radiation. In another case, NGC 3227, the apparently broad, asymmetric line profile (Pounds *et al.* 1989) has been interpreted as evidence for substantial gravitational and Doppler shifts, again arising from reprocessing close to the central black hole (George, Nandra & Fabian 1990). Finally, the strengths of the observed lines in most AGN (equivalent widths  $\sim 100\text{--}200$  eV) indicate that the reprocessing material subtends a large solid angle at the primary X-ray source.

Several workers have presented evidence for variability of AGN X-ray spectra. Often, this spectral variability is parameterized by a change in the power-law index (e.g. 3C120, Halpern 1985; NGC 4051, Lawrence *et al.* 1985; NGC 7314, Turner 1987; MCG-6-30-15, Matsuoka *et al.* 1990). The complex nature of the spectra as outlined above, now makes such a parameterization at best inadequate. However, in the case of NGC 4151, a careful recent analysis of new *Ginga* data has provided evidence for intrinsic spectral index variability, correlated with flux (Yaqoob & Warwick 1991). In some cases, flux-correlated variability, particularly in the low-energy region of the spectrum, has been interpreted as arising from changes in the ionization state of a variable (photo-ionized) absorber in the line-of-sight (Halpern 1984; Pan, Stewart & Pounds 1990). Detections of substantial 'warm' iron absorption edges by Nandra *et al.* (1990) and Pounds *et al.* (1990) lend support to such an interpretation. In these latter two cases, a composite model, consisting of X-ray reflection and fluorescence in cold material, together with a photo-ionized absorber, was preferred.

NGC 5548 is a bright Seyfert I galaxy of moderate luminosity [ $L_x(2\text{--}10\text{ keV}) \sim 10^{44}$  erg s $^{-1}$ ] at a redshift of 0.017. It has been observed with all the major X-ray missions and seen to be variable by a factor of up to 10 on long time-scales (see Hayes *et al.* 1980, and references therein). *EXOSAT* database for this object, comprising 12 observations close to the 'canonical' value ( $\Gamma \sim 1.7$ ), but with a substantial excess of photons at energies  $< 2$  keV (Branduardi-Raymont 1986; Turner & Pounds 1989; Kaastra & Barr 1989). Evidence has also been reported for spectral variability, in the usual sense that the 2–10 keV spectrum softens as the source brightens (Branduardi-Raymont 1989), and for a delay of  $\sim 1\text{--}2$  hr between variations in the hard and soft X-ray fluxes (Kaastra & Barr 1989). More recently an iron *K*-shell emission line, first observed in an *Ariel V* observation (Hayes *et al.* 1980), but in none of the subsequent observations, has been confirmed by *Ginga* (Pounds *et al.* 1989).

Here we present the analysis of multiple *Ginga* observations of NGC 5548 together with a re-analysis of the entire *EXOSAT* database for this object, comprising 12 observations with the *EXOSAT* ME and LE detectors. We find that an emission line, attributed to cold iron, is present in all the *Ginga* data. In addition, we confirm and better quantify the spectral variability first reported from the *EXOSAT* data. We conclude that the soft excess, iron line and spectral variability can be explained if a power-law source of X-rays illuminates a larger region of cold, optically thick material, with the spectrum being further modified by highly ionized material in the line-of-sight.

**Table 1.** Log of *Ginga* observations of NGC 5548.<sup>a</sup>

	Start date	Duration	Count rate (2–10 keV)
	UT	(s)	cts s $^{-1}$
1.	1988/176	120000	18.6 $\pm$ 0.1
2.	1989/009	76000	12.4 $\pm$ 0.1
3.	1989/028	140000	22.2 $\pm$ 0.1
4.	1989/159	51000	17.1 $\pm$ 0.1
5.	1989/194	60000	23.9 $\pm$ 0.1

<sup>a</sup>Errors in this and subsequent tables are  $1\sigma$ .

## 2 OBSERVATION LOG AND BACKGROUND MODELLING

### 2.1 The *Ginga* observations

A total of five observations of NGC 5548 were made in 1988/89 using the LAC (Turner *et al.* 1989) aboard *Ginga* (Makino *et al.* 1987), four of which coincided with a major *IUE*/multi-waveband campaign. Table 1 shows the observing log together with the 2–10 keV integrated count rates. The background was subtracted by the now standard techniques, using several blank sky observations to model systematic trends in the particle background levels, and hence to estimate the background level at the time of each source observations (Hayashida *et al.* 1989). In each case, data were taken only from the top-layer of the LAC as the so called 'mid-layer', whilst having a larger effective area above  $\sim 10$  keV, is subject to greater uncertainty in background estimation. In addition, contamination due to fluorescence by silver atoms in the collimator led to an unacceptable background subtraction around 22–25 keV. For this reason, our analysis was restricted to the 2–20 keV energy range. In one case (Observation 2) the pointing direction of the satellite was such that solar X-rays were able to enter the LAC for part of the observations, causing a large excess soft flux. These periods were therefore excluded.

### 2.2 The *EXOSAT* observations

Here we present a uniform analysis of all 12 *EXOSAT* observations of NGC 5548. Several of these observations have been reported previously (Branduardi-Raymont 1986, 1989; Turner & Pounds 1989; Kaastra & Barr 1989). Table 2 shows the observing log and count rates for the *EXOSAT* observations. In each case, data were accumulated using the ME proportional counters (2–10 keV) and the LE telescope with Channel Multiplier Array (CMA) in the focal plane. The 3000-Å Lexan (3 Lx), Aluminium/Parylene (Al/Pa) and Boron (B) filters were used in rotation within each observation, to derive spectral information from the CMA. The 4000-Å Lexan (4 Lx) filter was placed in the focal plane for part of two observations, but these data are excluded for consistency in the present work. In most cases, the ME background was determined from simultaneous blank sky observations using the offset detectors. Otherwise, the ME background was estimated from data collected when the

**Table 2.** Log of *EXOSAT* observations of NGC 5548.

	Start date	Duration	ME (2–10 keV)	3Lx	Al/Pa	B
	UT	(s)	cts s <sup>-1</sup>	10 <sup>-2</sup> cts s <sup>-1</sup>	10 <sup>-2</sup> cts s <sup>-1</sup>	10 <sup>-2</sup> cts s <sup>-1</sup>
1.	1984/032	14000	2.95 ± 0.08	16.1 ± 0.8	6.1 ± 0.8	1.3 ± 0.3
2.	1984/062	29000	4.87 ± 0.06	31.1 ± 0.5	12.7 ± 0.7	3.2 ± 0.4
3.	1984/141	34000	2.20 ± 0.04	29.4 ± 0.7	10.4 ± 0.5	2.1 ± 0.2
4.	1984/193	27000	3.04 ± 0.04	22.1 ± 0.4	8.8 ± 0.4	1.3 ± 0.2
5.	1985/014	19000	4.67 ± 0.06	25.2 ± 0.9	10.0 ± 0.5	2.2 ± 0.3
6.	1985/062	20000	3.83 ± 0.06	22.7 ± 0.8	8.8 ± 0.5	1.4 ± 0.2
7.	1985/159	20000	1.55 ± 0.06	3.2 ± 0.4	1.6 ± 0.2	< 0.3
8.	1985/173	15000	3.27 ± 0.07	8.3 ± 0.5	4.2 ± 0.4	0.6 ± 0.3
9.	1985/186	18000	1.74 ± 0.06	2.3 ± 0.4	1.2 ± 0.3	0.4 ± 0.2
10.	1985/195	14000	1.38 ± 0.07	3.2 ± 0.4	0.9 ± 0.3	< 0.4
11.	1986/019	44000	5.36 ± 0.04	31.6 ± 0.3	11.0 ± 1.0	2.0 ± 0.3
12.	1986/062	59000	4.18 ± 0.04	26.6 ± 0.2	11.0 ± 0.9	2.6 ± 0.4

satellite was slewing on or off source. The LE count rates were extracted using a  $100 \times 100$  arcsec<sup>2</sup> cell centred on the source and subtracting the background count rate, estimated from a concentric  $300 \times 300$  arcsec<sup>2</sup> box of blank sky. Appropriate corrections for dead-time and for scattering in the filters were applied.

### 3 X-RAY FLUX VARIABILITY

Long-term X-ray light curves of NGC 5548 are shown in Fig. 1. Variations of a factor of  $\sim 4$  are evident in the 2–10 keV X-ray flux on a time-scale of months. Over the period of the *EXOSAT* observations, the 3 Lx (0.5–2.0 keV) flux, although generally correlated with the ME level, varied with a much greater amplitude (factor  $\sim 14$ ). Unfortunately, no information in the soft ( $< 2$  keV) band is available with

*Ginga*. Kaastra & Barr (1989) have reported rapid ( $\sim$  few hours) variability in both the LE and ME flux from this object. Our analysis confirms this, with low-amplitude variability apparent in two of the five *Ginga* observations. Fig. 2 shows the 2–10 keV light curve of the 1989/159 observation, in which the flux varies by  $\sim 30$  per cent over a few hours. In addition, Kaastra & Barr reported evidence for a lag of the ME (2–8 keV) flux, compared to the 3 Lx (0.5–2.0 keV), based on one ‘event’ in the 86/062 data. In Fig. 3 we show the cross-correlation of the ME with the LE flux, for this observation. The function peaks at around 10 000 s indicating a lag of the hard flux with respect to the soft in agreement with the findings of Kaastra & Barr. Unfortunately the signal-to-noise ratio is too poor to allow confirmation of this behaviour in the other *EXOSAT* observations.

## 4 PRELIMINARY SPECTRAL ANALYSIS

### 4.1 Spectral index

The details of simple power-law fits to the *EXOSAT* ME data in the 2–10 keV band (with absorption by cold, cosmic abundance material; Morrison & McCammon 1983) are shown in Table 3. Although there is a suggestion of a trend, with the spectral index steepening as the source brightens (Fig. 4a), there is no statistically significant correlation [ $\chi^2 = 1.2$  for 12 degrees of freedom (dof) against a constant-index hypothesis]; the measurements are consistent with the weighted mean value of  $1.62 \pm 0.02$ . The corresponding *Ginga* fits, in the 2–20 keV range are shown in Table 4, where it can be seen that a simple power-law model does not provide a satisfactory fit to four of the five *Ginga* observations. However, using such a model as a simple parameterization of the spectral form in order to test for spectral variability, as suggested by the *EXOSAT* data, we find that

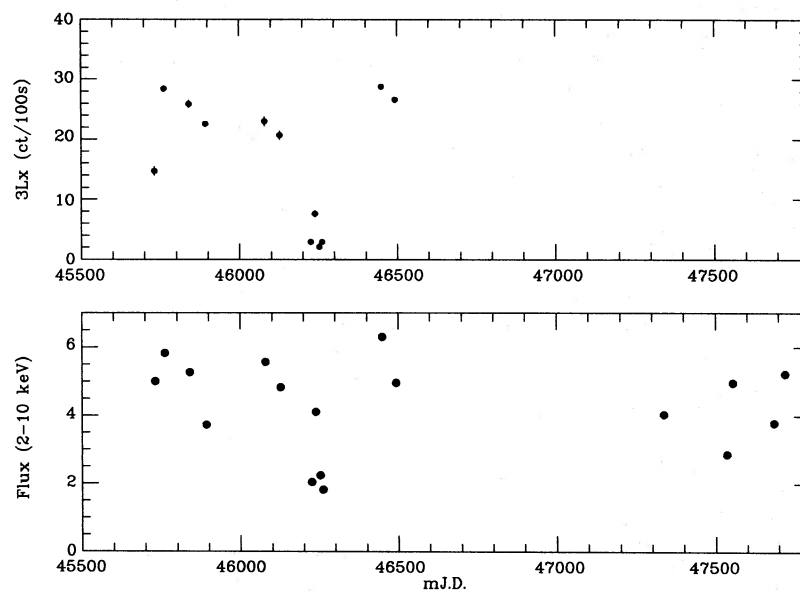


**Figure 1.** Long-term light curves of NGC 5548. The 2–10 keV (*EXOSAT* and *Ginga*) flux, measured in units of  $10^{-11}$  erg cm<sup>-2</sup> s<sup>-1</sup> is shown in the lower panel and varies by a factor of  $> 3$ . The *EXOSAT* CMA/3Lx (upper panel) count rate varies by a factor of  $\sim 14$ . Errors on the 2–10 keV flux are smaller than the symbols shown. The fluxes in the two bands are correlated, but the LE varies with a much larger amplitude.

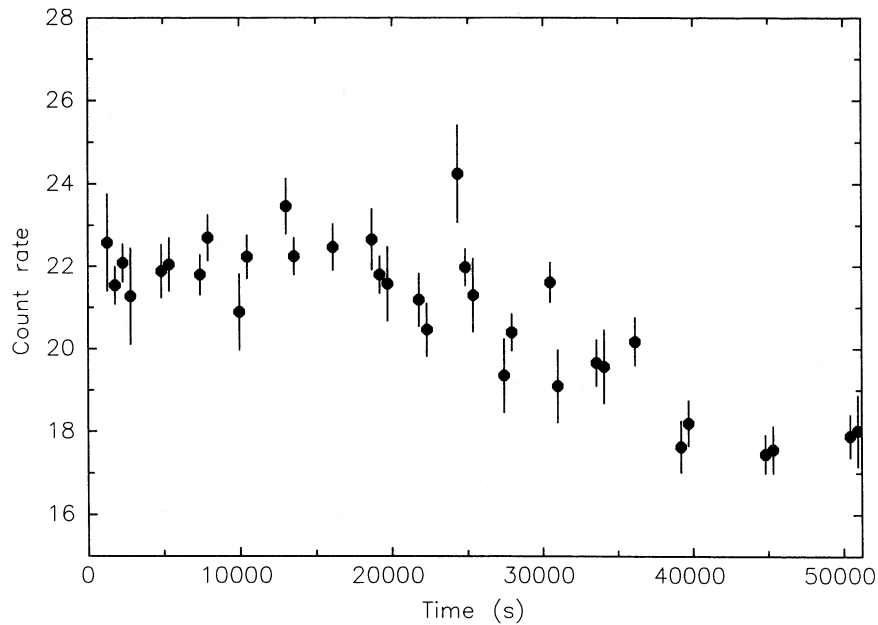


**Figure 2.** The 2–10 keV light curve obtained by *Ginga* on 1989/159. A 30 per cent decrease in the count rate occurs in a few hours.

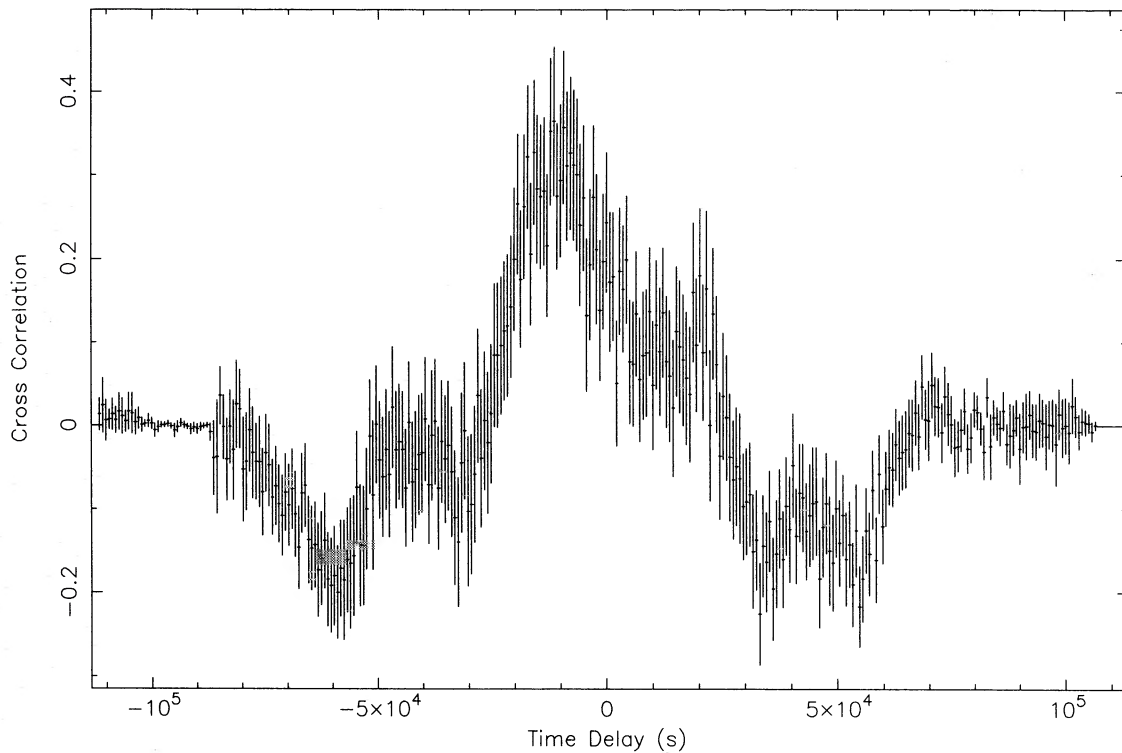


**Figure 3.** Cross-correlation of the ME and LE count rates from the 1986/062 *EXOSAT* observation. The lag first reported by Kaastra & Barr (1989) of  $\sim$  few hr is confirmed.

the apparent spectral index changes significantly between individual *Ginga* observations, but is not obviously correlated with flux (Fig. 4b). Comparable behaviour has been reported for 3C273 (Turner *et al.* 1990). Also shown in Table 4 is the power-law fit in the 10–20 keV energy range.

The indices derived from these fits are flatter than those from the wider energy band, indicating a ‘hard tail’ to the data. The weighted mean index from the 10–20 keV fits,  $\Gamma = 1.37 \pm 0.10$ , is inconsistent with the 2–20 keV mean,  $\Gamma = 1.66 \pm 0.02$ .

**Table 3.** Power-law fits to the *EXOSAT* ME (2–10 keV) data.<sup>a</sup>

	Norm <sup>b</sup> 10 <sup>-2</sup> ph s <sup>-1</sup> cm <sup>-2</sup>	Photon index Γ	N <sub>H</sub> 10 <sup>21</sup> cm <sup>-2</sup>	F <sub>2-10</sub> erg s <sup>-1</sup> cm <sup>-2</sup>	χ <sub>r</sub> <sup>2</sup> /d.o.f.
1.	0.8	1.45 ± 0.10	0.0 <sup>+1.6</sup> <sub>-0.0</sub>	5.00 ± 0.10	0.86/32
2.	1.5	1.75 ± 0.07	0.0 <sup>+1.6</sup> <sub>-0.0</sub>	5.83 ± 0.07	1.14/32
3.	1.3	1.68 ± 0.06	0.0 <sup>+1.6</sup> <sub>-0.0</sub>	5.27 ± 0.06	0.79/32
4.	0.8	1.58 ± 0.06	0.0 <sup>+2.5</sup> <sub>-0.0</sub>	3.73 ± 0.05	0.94/32
5.	1.4	1.69 ± 0.10	1.4 <sup>+3.2</sup> <sub>-1.4</sub>	5.56 ± 0.07	0.98/32
6.	1.4	1.76 ± 0.12	5.6 <sup>+3.2</sup> <sub>-2.6</sub>	4.74 ± 0.07	1.63/32
7.	0.3	1.28 ± 0.18	0.0 <sup>+4.6</sup> <sub>-0.0</sub>	2.04 ± 0.08	0.82/32
8.	0.8	1.50 ± 0.16	1.8 <sup>+5.2</sup> <sub>-1.8</sub>	4.12 ± 0.09	1.26/32
9.	0.4	1.50 ± 0.27	3.6 <sup>+9.4</sup> <sub>-3.6</sub>	2.23 ± 0.08	0.82/32
10.	0.3	1.40 ± 0.30	1.2 <sup>+11.2</sup> <sub>-1.2</sub>	1.83 ± 0.05	0.73/32
11.	1.5	1.64 ± 0.03	0.0 <sup>+1.4</sup> <sub>-0.0</sub>	6.38 ± 0.05	1.42/32
12.	1.1	1.61 ± 0.03	0.0 <sup>+0.7</sup> <sub>-0.0</sub>	4.96 ± 0.05	1.28/32

<sup>a</sup>Errors calculated in the spectral fitting procedure are 68 per cent confidence ( $1\sigma$ ) with one parameter of no interest; <sup>b</sup>flux at 1 keV; <sup>c</sup>corrected for absorption.

**Table 4.** Power-law fits to the *Ginga* data.

Energy Range	Norm 10 <sup>-2</sup> ph s <sup>-1</sup> cm <sup>-2</sup>	Photon index Γ	N <sub>H</sub> 10 <sup>21</sup> cm <sup>-2</sup>	F <sub>2-10</sub> erg s <sup>-1</sup> cm <sup>-2</sup>	χ <sub>r</sub> <sup>2</sup> /d.o.f.
1. 2–18	1.0	1.70 ± 0.02	0.0 <sup>+0.1</sup> <sub>-0.0</sub>	4.34 ± 0.02	1.84/24
2. 2–18	0.5	1.43 ± 0.07	12.1 <sup>+3.7</sup> <sub>-3.5</sub>	3.23 ± 0.04	1.21/24
3. 2–18	1.0	1.55 ± 0.03	4.1 <sup>+1.3</sup> <sub>-0.9</sub>	5.55 ± 0.02	1.81/24
4. 2–18	0.8	1.60 ± 0.03	0.9 <sup>+1.5</sup> <sub>-0.9</sub>	4.64 ± 0.02	1.45/24
5. 2–18	1.4	1.72 ± 0.02	1.2 <sup>+1.0</sup> <sub>-0.6</sub>	5.81 ± 0.02	2.71/24
1. 10–18	0.6	1.44 ± 0.12	–	–	0.5/16
2. 10–18	0.4	1.40 ± 0.28	–	–	0.5/16
3. 10–18	0.4	1.23 ± 0.13	–	–	0.6/16
4. 10–18	0.7	1.56 ± 0.15	–	–	1.1/16
5. 10–18	0.5	1.31 ± 0.11	–	–	1.3/16

<sup>a</sup>Corrected for absorption.

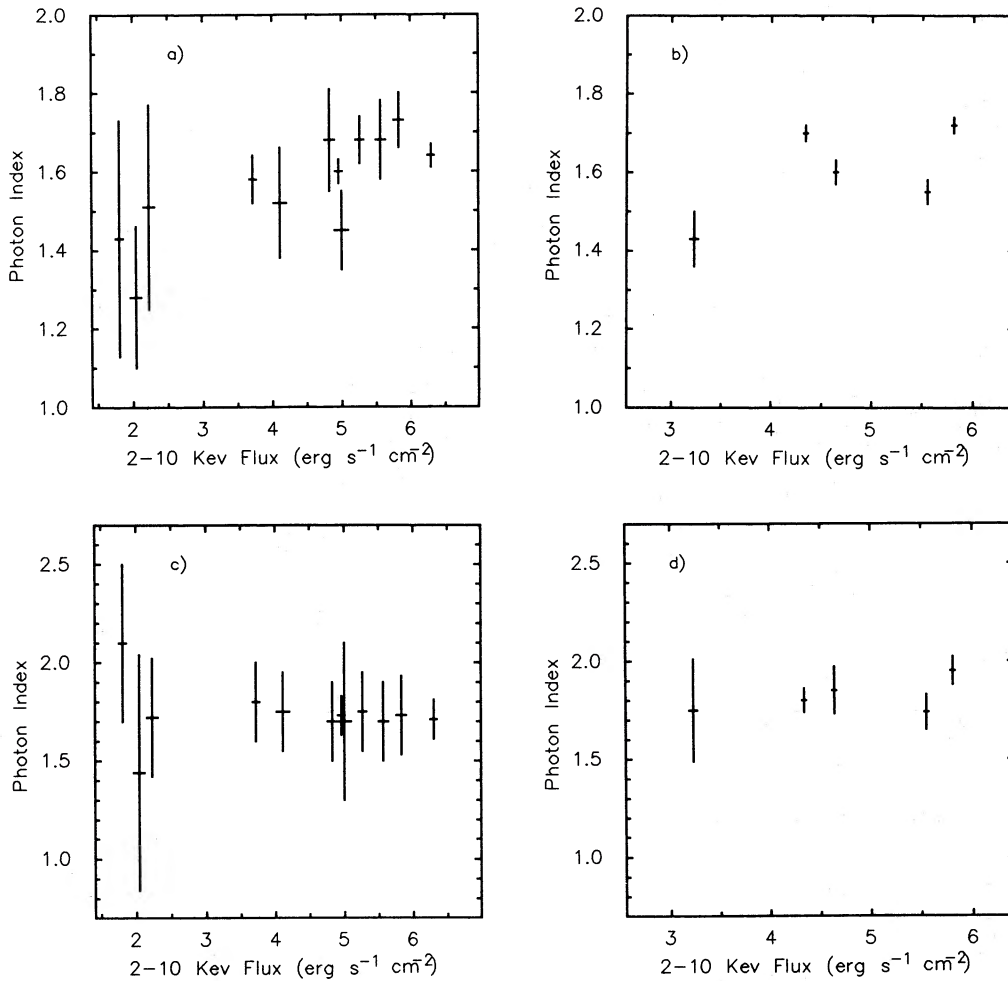


**Figure 4.** Flux versus apparent photon index plots for the *EXOSAT* (left panels) and *Ginga* (right panels) data. The changes in the *EXOSAT* slope are not statistically significant. However, the *Ginga* simple power-law fits (upper plot) show significant changes in index, apparently uncorrelated with the flux. When an accretion disc reflection component, with  $i = 30^\circ$ , is included (lower plots), the intrinsic index is consistent with a constant,  $\Gamma = 1.83$ . Similar results are obtained for  $i = 60^\circ$ , although the implied intrinsic index is somewhat steeper ( $\Gamma = 1.91$ ).

**Table 5.** Line parameters for NGC 5548.

Photon index	Line flux $10^{-4}$ ph $s^{-1}$ $cm^{-2}$	Equivalent Width eV	Energy keV	$\chi^2/d.o.f.$	$\sigma^a$ keV
1. $1.71 \pm 0.02$	$0.34 \pm 0.21$	$80 \pm 50$	$6.4 \pm 0.4$	1.40/23	$< 0.9$
2. $1.44 \pm 0.09$	$0.87 \pm 0.45$	$250 \pm 130$	$6.2 \pm 0.3$	0.57/23	$< 2.0$
3. $1.57 \pm 0.04$	$0.60 \pm 0.28$	$110 \pm 50$	$6.1 \pm 0.5$	1.03/23	$0.8^{+0.9}_{-0.5}$
4. $1.62 \pm 0.05$	$0.58 \pm 0.17$	$140 \pm 70$	$6.2 \pm 0.4$	0.67/23	$< 1.1$
5. $1.74 \pm 0.03$	$0.72 \pm 0.22$	$130 \pm 40$	$6.3 \pm 0.2$	0.84/23	$< 0.9$

<sup>a</sup> $\sigma$  of Gaussian obtained from a fit with finite line width.

## 4.2 Iron line emission

We find that a spectral model comprising of a power law plus narrow Gaussian emission line gives significantly improved fits (at  $>99$  per cent confidence using the F-test) for all five *Ginga* observations (Table 5). In one case (observation 3) the fit requires a finite line width (significant at the  $\sim 99$  per cent level); upper limits to the line width are given for the other four observations (Table 5, final column). The implied equivalent width for this broad line,  $\sim 200$  eV, is somewhat larger than the narrow line. In all cases the derived line energy is close to 6.4 keV and the line has a mean equivalent width of  $130 \pm 40$  eV. In contrast, in only one of the *EXOSAT* observations (86/062) is there a statistical requirement for the inclusion of an emission line at 6.4 keV to the simple power-law model. The derived equivalent width for this observation is similar to that above. It should be noted, however, that none of the *EXOSAT* observations exclude the existence of an emission line of this strength and if all the ME spectral data are summed, a line is detected with an equivalent width of  $\sim 110$  eV. The *EXOSAT* data are therefore entirely consistent with the *Ginga* line measurements.

The weighted mean of the *Ginga* line energies (in the rest frame of NGC 5548),  $6.31 \pm 0.13$  keV, excludes recombination or fluorescence from highly ionized iron atoms as the origin of the line, assuming that the energy of the emission

line remains constant. Although variability of the line equivalent width is suggested (e.g. by comparison of *Ginga* observations 1 and 2), it is not possible to statistically exclude the hypothesis that either the line flux, or the equivalent width stays constant.

## 4.3 Absorbing column densities

From Tables 3 and 4, it can be seen that the low-energy absorbing column density in NGC 5548 is variable between individual observations. Note that the column densities,  $N_H$ , derived from the *EXOSAT* data given in Table 4 are from the ME data alone since the ME plus LE data are susceptible to confusion by the soft X-ray excess (see Section 7.3). However, the interpretation of  $N_H$  is somewhat model dependent and is discussed more fully in Section 5.

## 5 TRANSMISSION MODELS

Transmission of X-rays through neutral, or partially ionized gas results in fluorescent line emission. Indeed, as stated above, the measured X-ray column densities in the heavily obscured sources NGC 4151 and Cen A are sufficient to explain the line emission by fluorescence in a spherical shell. As has been stated previously (Pounds *et al.* 1989), however, it would appear that the measured soft X-ray absorption column density along the line-of-sight to NGC 5548 ( $N_H \sim 10^{21-22}$   $cm^{-2}$ ) is insufficient to explain the observed equivalent width of the iron line. We have carried out Monte Carlo calculations, similar to those described in Inoue (1985) and Makishima (1986) to verify this. Photons from a power-law source with  $\Gamma=1.7$ , embedded in the centre of a spherical gas cloud, are followed until they emerge from the cloud or are absorbed. Thus, the fluorescent line equivalent width can be calculated as a function of covering column density. The dominant radiative process is bound-free absorption (possibly followed by fluorescence); however, Compton scattering has a small effect and is included.

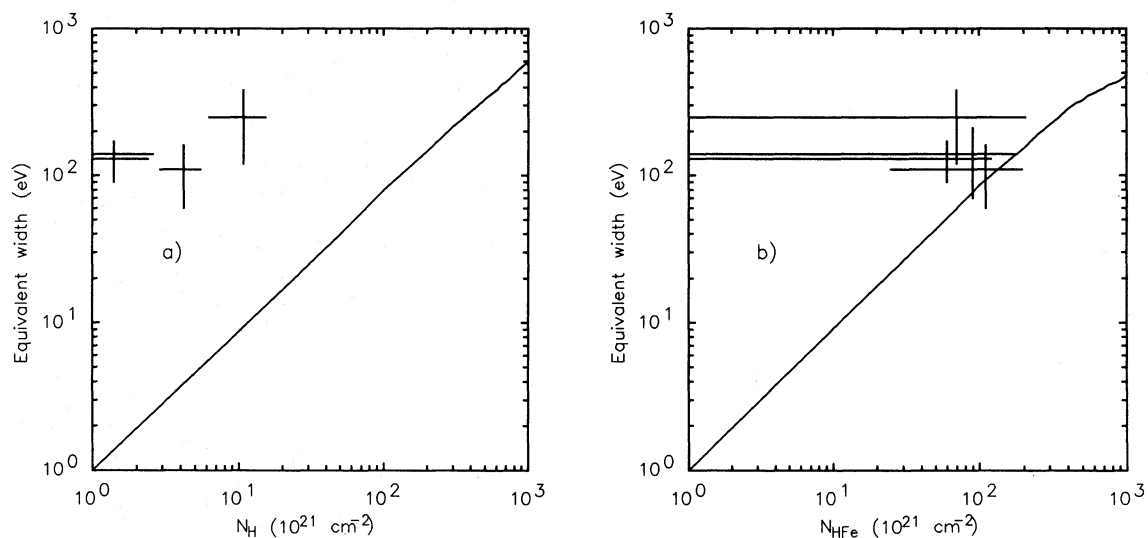


**Figure 5.** Measured column densities versus equivalent width. In the left panel, the solid line is the Monte Carlo prediction assuming full spherical coverage by a cold column. The measured soft X-ray columns,  $N_H$ , are clearly insufficient to explain the line strength; however, the iron column density,  $N_{Fe}$ , derived from a fit to an iron edge at  $\sim 8$  keV (right panel) may be sufficient to provide a significant proportion of the observed line flux. Here the Monte Carlo model assumes highly ionized material.

### 5.1 A cold spherical shell

A plot of the observed equivalent widths versus measured low-energy column density for the five *Ginga* observations is shown in Fig. 5(a). The solid line is the Monte Carlo prediction, assuming complete spherical covering by cold cosmic abundance gas (Morrison & McCammon 1983) with hydrogen column density  $N_{\text{H}}$ . It can be seen that the measured values of the equivalent width are considerably in excess of those predicted by spherical covering with the measured  $N_{\text{H}}$ .

However, a highly ionized medium would be transparent at soft X-ray energies (2–3 keV) and may lead us to considerably underestimate the line-of-sight column density during the spectral fitting. We now consider the possibility that this highly ionized gas provides the observed spectral features.

### 5.2 A photo-ionized absorber

The substantial flux of ionizing photons from the active nucleus will lead to photo-ionization of the line-of-sight material. We have approximated a case of extreme photo-ionization by assuming all electrons have been stripped, except for iron *K*. Here we define  $N_{\text{HFe}}$  as the column density of iron divided by the cosmic abundance of iron.  $N_{\text{HFe}}$  therefore represents the equivalent hydrogen column density. The fluorescence yield,  $\omega_{\text{K}}$  (defined as the probability that the atom de-excites via a radiative transition rather than the Auger process), in this ionization state (Fe xxv – helium like iron), is  $\sim 0.5$ , compared to  $\omega_{\text{K}} \sim 0.3$  for cold iron (Krolik & Kallman 1987, and references therein). Accounting for this, the fluorescence line from the highly ionized gas can be calculated as above. Note that in the optically thin case, the increase in  $\omega_{\text{K}}$  leads to a larger equivalent width for a column  $N_{\text{HFe}}$ , compared to the corresponding cold  $N_{\text{H}}$ . As this material has no effect at low X-ray energies, our only observational measure of the column density comes from the imprint left at the iron *K*-edge at 7–9 keV.

In Table 6 we list the parameters of a spectral model consisting of a power law, a narrow emission line (fixed at 6.4 keV) and such an edge when applied to the *Ginga* data. We have performed fits with edge energies fixed at 7.1 keV (cold iron), 8.85 keV (helium-like iron) and 8.0 keV (representing an intermediate-ionization stage  $\sim$  Fe xx). Examining derived values of  $N_{\text{HFe}}$  and  $\Delta\chi^2$  we conclude that there is no evidence for a helium-like edge. Two of the five observations, however, show evidence for an edge at lower X-ray energies. An edge at 7.1 keV, implying cold material, seems unlikely as in the cases where such an edge is allowed this would imply an iron abundance of  $\sim 20$  and  $\sim 100$  times the cosmic values (for observations 3 and 4, respectively). An edge at 8

keV is more likely, although it is possible that such a feature could merely represent an artefact of the complex spectral model described below. We plot the values of  $N_{\text{HFe}}$  derived from these fits at 8 keV against our Monte Carlo prediction for highly ionized material in Fig. 5(b). It can be seen that the theoretical curve still falls short of the measured equivalent widths. The line energy of *K*-shell fluorescence from Fe xx is  $\sim 6.5$  keV (Makishima 1986), just incompatible with the observed line energy. Although the warm absorber cannot provide a full explanation for the observed spectrum, we conclude it may contribute to both absorption and emission features. This is considered further in Section 7.

### 5.3 Partial covering

If the absorber is cold but non-uniform, which has been suggested to explain the complex low-energy X-ray spectrum of NGC 4151 (e.g. Yaqoob & Warwick 1991), this could again confuse our measurement of  $N_{\text{H}}$ . We have tested such a cold partial covering model, including a 6.4-keV emission line, against our *Ginga* data. Since poor constraints are obtained when both the covering fraction and partially covering column are left free, we have conducted fits with the covering fraction fixed at several values. The results are summarized in Table 7. This partial covering model improves the fit to the data significantly over the power law plus line model in two out of the five *Ginga* observations, with a covering fraction of 25 per cent, and explains all the data adequately. Two problems exist with this model, however. First, the (apparently random) variability in the covering column, which parameterizes the spectral variability has little physical basis and secondly, the covering fraction ( $\sim 25$  per cent) is insufficient to alone provide the necessary iron fluorescence (and larger covering fractions are ruled out by the data: see Table 7).

Such a model, with  $N_{\text{H}} \geq 10^{23} \text{ cm}^{-2}$  as derived here, has recently been proposed to account for the high-energy tail observed in the X-ray spectra of several Seyferts (Piro, Matsuoka & Yamauchi 1990; Matsuoka *et al.* 1990). Whilst the hard tail could arise from transmission of hard X-rays through optically thick material, a more likely explanation is that the hard X-rays are predominantly reflected from such material, unless the covering fraction and column density lie in a small range, and are similar for many Seyferts. We conclude that this partial covering model is merely a crude parameterization of the effects of X-ray reflection from cold material described below.

Summarizing, none of the transmission models can alone provide an adequate description of the complex spectrum. This leads us to the conclusion that the bulk of the features arise in cool dense material out of the line-of-sight to the primary source of X-rays.

**Table 6.** Absorption edge fits.

	Energy	$N_{\text{HFe}}$	$\Delta\chi^2$	Energy	$N_{\text{HFe}}$	$\Delta\chi^2$	Energy	$N_{\text{HFe}}$	$\Delta\chi^2$
	keV	$10^{21} \text{ cm}^{-2}$		keV	$10^{21} \text{ cm}^{-2}$		keV	$10^{21} \text{ cm}^{-2}$	
1.	7.1	$10_{-10}^{+50}$	0.0	8.0	$0_{-0}^{+40}$	0.0	8.85	$0_{-0}^{+40}$	0.0
2.	7.1	$60_{-60}^{+150}$	0.8	8.0	$70_{-70}^{+200}$	0.6	8.85	$40_{-40}^{+280}$	0.1
3.	7.1	$70_{-70}^{+80}$	5.2	8.0	$110_{-90}^{+80}$	6.6	8.85	$80_{-80}^{+110}$	1.2
4.	7.1	$90_{-80}^{+70}$	6.4	8.0	$90_{-90}^{+90}$	4.1	8.85	$30_{-30}^{+140}$	0.2
5.	7.1	$40_{-40}^{+30}$	2.6	8.0	$60_{-60}^{+90}$	3.2	8.85	$50_{-50}^{+90}$	1.3

## 6 REFLECTION MODELS

The material producing the UV/soft X-ray ‘bump’ may well be optically thick and is a likely source for the iron fluorescence. The expected maximum in the continuum at  $\sim 30$  keV, produced by Compton down-scattering in such cold material (Lightman & White 1988) is then a probable source of the X-ray hard tail (Section 4.1).

The fact that the observed mean equivalent width ( $\sim 130$  eV) for NGC 5548, is near the maximum value for a reflective 'slab' behind an optically thin source ( $\sim 150$  eV; George & Fabian 1991), suggests that if such a slab is the only significant source of fluorescence line, it is viewed almost face-on and subtends a solid angle  $\sim 2\pi$  at the X-ray source. Alternatives to the geometry described here do exist, e.g. if the material was in the form of an accretion disc, expanded by its own radiation pressure into a saucer shape or conical geometry, or the illuminating X-ray source was anisotropic (see Ghisellini *et al.* 1991), then the viewing angle constraint would be relaxed somewhat.

As any major reprocessing region is likely to be larger than the primary X-ray source, the observed intensity of the fluorescence line will not instantly respond to variations in the illuminating X-ray flux, leading to variations in the observed equivalent width of the line. In addition, the albedo

of cold matter has a characteristic shape in the X-ray band (e.g. Lightman & White 1988; Fig. 6). Changes in the relative level of directly viewed to the Compton reflected continua, as a result of variability of the illuminating source, will therefore give rise to variability in the observed spectrum. For certain modes of variability (e.g. quasi-sinusoidal), if the time-scale for changes in the reflected component is longer than both the variability time-scale of the primary X-ray source and the duration of a typical spectral measurement, then an apparent flux-index correlation could result.

In order to test the hypothesis that the apparent variations in the X-ray spectral index in NGC 5548 are due to differential variability, we have used the Monte Carlo model described in George & Fabian (1991) to simulate the reflected continuum and fluorescence line expected from cold, optically thick material. Initially, a reflecting slab is assumed to lie behind a source isotropically emitting a

Table 7. Partial covering fits.

	Coverage	$N_{\text{H}}$	$\Delta\chi^2$		$N_{\text{H}}$	$\Delta\chi^2$	Coverage	$N_{\text{H}}$	$\Delta\chi^2$
	%	$10^{21} \text{ cm}^{-2}$	%		$10^{21} \text{ cm}^{-2}$	%	$10^{21} \text{ cm}^{-2}$	%	
1.	25	$2100^{+1900}_{-1300}$	10.7	50	$0^{+2}_{-0}$	0.0	75	$0^{+2}_{-0}$	0.0
2.	25	$90^{+680}_{-90}$	1.3	50	$40^{+80}_{-40}$	1.3	75	$16^{+12}_{-16}$	0.4
3.	25	$240^{+180}_{-240}$	7.0	50	$10^{+6}_{-10}$	1.3	75	$5^{+3}_{-5}$	0.2
4.	25	$3500^{+34000}_{-2600}$	2.0	50	$1^{+7}_{-1}$	0.0	75	$0^{+4}_{-0}$	0.0
5.	25	$6000^{+\infty}_{-3000}$	1.9	50	$2^{+3}_{-0}$	0.0	75	$0^{+4}_{-0}$	0.0

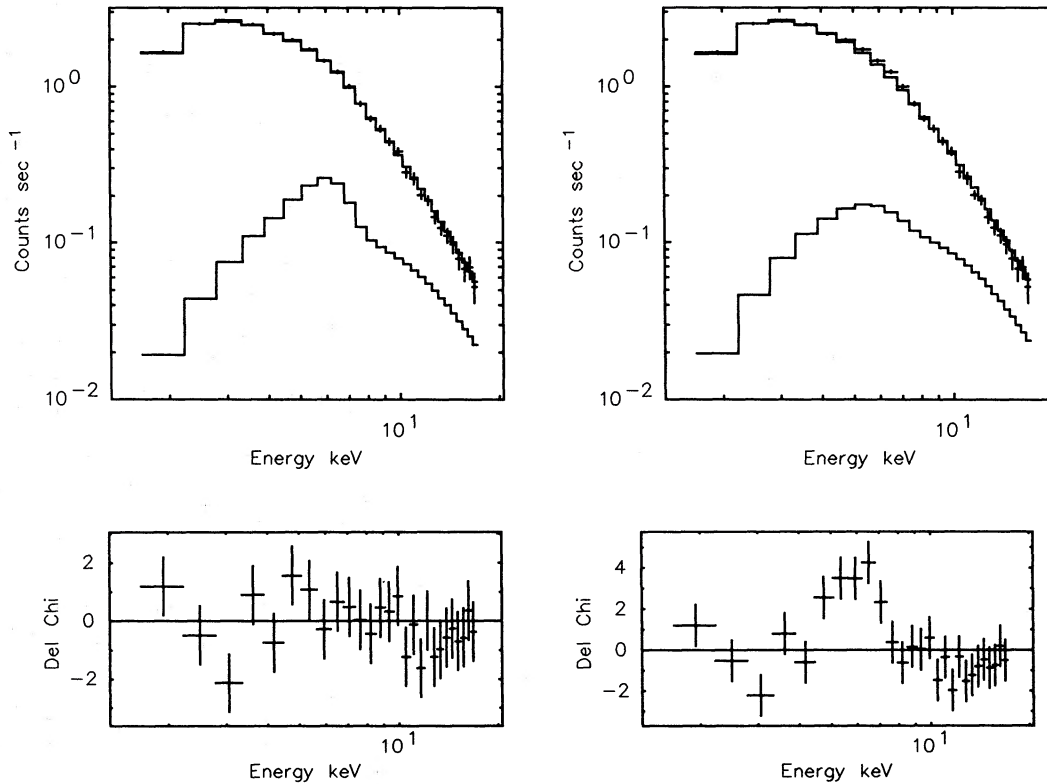


Figure 6. Best-fit counts spectrum and residuals (left panels) for a composite fit, including an accretion disc reflection component fixed at  $i = 60^\circ$ , to the *Ginga* PHA spectrum of NGC 5548 (1989/028). The disc reflection component, plotted separately, clearly shows the line and hard tail. The model iron line is significantly broadened by Doppler, gravitational and Compton effects, as illustrated in the residuals when the line is removed (right panels).

power-law X-ray spectrum. Photons are injected from this source into the reflecting medium and are followed until they either re-emerge after Compton scattering or fluorescence or are absorbed. Both Fe  $K\text{-}\alpha$  ( $\sim 6.4$  keV) and  $K\text{-}\beta$  ( $\sim 7.1$  keV) are included, along with Ni  $K\text{-}\alpha$  ( $\sim 8.3$  keV). The only line-broadening process included thus far is Compton scattering (which dominates over, e.g. thermal broadening), which is not significant when compared to the resolution of the LAC. The line equivalent width is a strong function of the inclination,  $i$ , of the observer relative to the normal to the slab, due to the reduction in projected area as  $i \rightarrow 90^\circ$  (edge-on) and the increased path length through the absorbing medium for photons escaping at grazing angles.

### 6.1 Cold matter far from the nucleus

The results of spectral analysis of the *Ginga* data using this slab reflection model are shown in Table 8. This model is only physically realistic if the reflecting material lies far from the nucleus, for example in the form of an accretion torus as described by Antonucci & Miller (1985), such that there is no significant line broadening. Although the reflected luminosity depends in detail on the geometry of the cold material, the spectral form of the reflected continuum is virtually constant. We have therefore arbitrarily chosen an inclination,  $i = 30^\circ$  for the slab. Statistically acceptable fits are obtained for all the *Ginga* data. In particular, *Ginga* observation 1, for which the ‘power law plus line’ fit was previously unacceptable, shows a greatly improved fit, indicating that the continuum curvature inherent in the reflection model is strongly preferred.

### 6.2 A Keplerian accretion disc

The reprocessing matter may well lie sufficiently close to the black hole for Doppler and gravitational effects to significantly broaden the fluorescent emission line. The fact that one of the observation shows, and the others are compatible

with, such a broad line suggests that much of the material does indeed lie close to the central hole. Whilst the geometry is unclear, either an accretion disc, or a ‘mist’ of small, dense cloudlets (as described by Guilbert & Rees 1988) are both plausible. We note that such optically thick cloudlets close to the X-ray source would produce a similar effect to that of the accretion disc model considered here, as long as the solid angle subtended at the power-law source is large. Here we consider a geometrically thin, optically thick accretion disc, assumed dense enough to remain in a low state of ionization despite the intense hard photon flux.

The surface emissivity of the disc reflection was calculated as a function of radius, according to the prescription of George & Fabian (1991). Power-law fits to this emissivity function can then be used in conjunction with the formulae of Chen, Halpern & Filippenko (1989) to include a detailed calculation of the line profile. These formulae include gravitation (in the weak gravity approximation) and Doppler effects.

The equivalent width of the line observed in NGC 5548 is of a similar order to that expected from a face-on accretion disc; however, the broad profile of the line may suggest a higher inclination. We have therefore fixed the disc inclination at two values,  $i = 30^\circ$  and  $i = 60^\circ$ . The main differences between these are the width of the line, due to the increased Doppler effect at higher inclination, and the luminosity of the reflected component relative to the incident X-rays, which falls with increasing inclination.

We find that the disc reflection model provides statistically acceptable fits to both the *EXOSAT* and *Ginga* data, with generally similar  $\chi^2_\nu$  to those obtained for the slab model. The parameters for the *EXOSAT* fits are not well constrained (see Fig. 4c), but the *Ginga* data show that the higher inclination ( $i = 60^\circ$ ) is preferred in the spectral fitting (note also the substantial improvement over the slab model for observation 3, which requires a broad line). Fig. 6 shows a typical count spectrum, with residuals, for one of the *Ginga* fits (1989/009). For clarity, the reflection component is plotted separately. The emission line is clearly seen (broadened in our reflection model by gravity, Compton and Doppler effects), as is the flattening due to the Compton reflection hump at high energies. The intrinsic spectral indices for all five *Ginga* observations (Table 8) are well constrained and consistent with weighted mean values of  $1.84 \pm 0.06$  ( $\chi^2_r = 0.7$ ) and  $1.91 \pm 0.07$  ( $\chi^2_r = 0.8$ ) for  $i = 30^\circ$  (shown in Fig. 4d) and  $i = 60^\circ$ , respectively. These are both fully consistent with those derived from the *EXOSAT* data (Fig. 4c), and again are significantly higher than in previous simple power-law fits.

Comparison of columns 3 and 4 in Table 8 reveals that the normalization of the reflected component varies with similar amplitude as the directly viewed continuum. Although statistically the normalization of the reflected continuum is consistent with a constant value, we note that both the relative and absolute amplitude of this component must change, otherwise a simple flux–index correlation would result from simple power-law fits, contrary to our observations (Table 4 and Fig. 4a).

#### 6.2.1 Constraints on the disc inclination

One puzzling aspect of the above reflection fits is that of the preferred disc inclination. For the  $i = 30^\circ$  case, the average

**Table 8.** Reflection fits to the *Ginga* data.

Model	$i$	$\Gamma$	$N_{\text{H}}$ $10^{21} \text{ cm}^{-2}$	Direct <sup>a</sup> norm	Ref. norm	Rel. norm	$\chi^2/\text{d.o.f.}$	
1.	Slab	30	$1.78 \pm 0.04$	$0.0^{+0.9}_{-0.0}$	$1.10 \pm 0.06$	$0.62 \pm 0.28$	0.56	0.87/23
2.	Slab	30	$1.70 \pm 0.19$	$15.5^{+5.4}_{-4.7}$	$0.71 \pm 0.18$	$1.08 \pm 0.84$	1.52	0.69/23
3.	Slab	30	$1.69 \pm 0.07$	$6.2^{+1.6}_{-1.6}$	$1.22 \pm 0.12$	$0.74 \pm 0.42$	0.61	1.21/23
4.	Slab	30	$1.77 \pm 0.09$	$3.3^{+2.4}_{-1.8}$	$1.02 \pm 0.15$	$0.84 \pm 0.54$	0.82	0.65/23
5.	Slab	30	$1.87 \pm 0.06$	$3.5^{+1.5}_{-0.9}$	$1.67 \pm 0.15$	$1.22 \pm 0.63$	0.73	1.10/23
1.	Disc	30	$1.80 \pm 0.06$	$0.0^{+1.3}_{-0.0}$	$1.12 \pm 0.08$	$1.08 \pm 0.62$	0.96	0.89/23
2.	Disc	30	$1.75 \pm 0.26$	$15.5^{+6.0}_{-4.1}$	$0.74 \pm 0.26$	$1.93 \pm 3.18$	2.61	0.76/23
3.	Disc	30	$1.74 \pm 0.09$	$6.6^{+2.0}_{-1.6}$	$1.29 \pm 0.09$	$1.55 \pm 0.97$	1.20	1.10/23
4.	Disc	30	$1.85 \pm 0.12$	$4.1^{+2.5}_{-1.9}$	$1.12 \pm 0.20$	$1.97 \pm 1.76$	1.76	0.55/23
5.	Disc	30	$1.95 \pm 0.07$	$4.4^{+1.2}_{-1.5}$	$1.83 \pm 0.20$	$3.10 \pm 1.68$	1.69	1.36/23
1.	Disc	60	$1.81 \pm 0.08$	$0.0^{+1.8}_{-0.0}$	$1.14 \pm 0.11$	$2.8 \pm 2.1$	2.5	0.86/23
2.	Disc	60	$1.94 \pm 0.29$	$16.8^{+4.4}_{-5.2}$	$0.91 \pm 0.38$	$9.8 \pm 7.0$	10.8	0.72/23
3.	Disc	60	$1.81 \pm 0.14$	$7.4^{+2.2}_{-2.0}$	$1.40 \pm 0.26$	$5.5 \pm 4.2$	3.9	0.93/23
4.	Disc	60	$1.96 \pm 0.13$	$4.8^{+2.3}_{-2.0}$	$1.25 \pm 0.23$	$8.0 \pm 5.2$	6.4	0.47/23
5.	Disc	60	$2.00 \pm 0.07$	$4.7^{+1.3}_{-0.9}$	$1.92 \pm 0.11$	$9.6 \pm 3.5$	5.0	0.98/23

<sup>a</sup>All normalizations are in units of  $10^{-2} \text{ ph cm}^{-2} \text{ s}^{-1}$ .

relative normalization between reflected and direct components is close to 1, suggesting that, for a disc-like geometry and a covering factor of  $2\pi$  as in our test model, this is the preferred value. However, it is clear from Table 8 that the higher inclination,  $i = 60^\circ$ , provides a statistically better fit to the data than in the face-on case. In this case the reflected normalization is, on average,  $\sim 6$  times greater than what would be expected for the time-averaged spectrum with a disc at this angle. Such a large discrepancy could not be accounted for by a conical disc, where the maximum increase relative to the slab case would be a factor of order 2. Anisotropic inverse Compton emission of the illuminating hard X-ray source, such as that described by Ghisellini *et al.* (1991) might account for this. However, a further problem with these highly inclined fits is the implied equivalent width, which ranges from  $\sim 150$  to  $\sim 750$  eV. Presumably these large equivalent widths are accommodated because of the broad profile of the line, the photons being ‘smeared’ over several *Ginga* bins, consistent with the broad Gaussian line fits (Table 5). The appropriate inclination of the disc is obviously crucial to a correct interpretation of the physical environment.

We have therefore investigated further the question of the disc inclination. As the shape of the reflected continuum is virtually independent of  $i$ , the main constraint comes from the properties of the emission line. Both the time-averaged equivalent width of the Fe *K*-line and its profile are functions of  $i$  and, therefore, two methods are available to quantify the inclination. The normalization of the reflected component can be fixed relative to the power-law normalization, whereby the value of  $i$  derived from the spectral fitting is primarily governed by the observed equivalent width. Alternatively, both the relative normalization and inclination can be left as free parameters in the spectral fitting, whereby the line profile will provide the only constraint on  $i$ .

We note that these two fits are necessarily geometry dependent. If a disc-like orientation of the cold material does not prevail, then these fits will be inappropriate. Also, if the

solid angle subtended by the disc at the X-ray source differs significantly from that of our test model ( $2\pi$ ) then the first method stated above will yield an incorrect value for  $i$ . It is also necessary to fit to a time-averaged spectrum, as significant time-lags between power law and line as described above would invalidate the fit. Therefore a fit to the summed data from the five *Ginga* observations was used. The first fit, with the disc contribution tied to the direct power law, gave an inclination,  $i = 45^\circ \pm 8^\circ$ . We note that this value is consistent with that of the host galaxy of NGC 5548, implied from the axial ratio ( $a/b = 0.83$ ; Keel 1980). The second fit, in which the line profile is the main constraint on the inclination, gave  $i = 80^\circ \pm 25^\circ$ , but with a normalization some 50 times larger than that expected from such an edge on disc. Although this fit represents a significant statistical improvement over the previous one, the anisotropic emission mechanism mentioned above could not account for such a large discrepancy. A possible explanation of this puzzling dilemma is that the accretion disc is in fact observed close to face-on, but is not the only source of fluorescent line emission. This possibility is taken up again in Section 7.2.

## 7 IMPLICATIONS OF THE MODELLING

### 7.1 Absorption

It is clear that the X-ray column measurements in the reflection model fits of Table 8 are not constant (this is also true for the simple power-law fits – see Section 4.3). The most obvious change in column occurs in the lowest-flux *Ginga* observation, with a column larger than all the other *Ginga* absorption measurements. Although these changes could arise from the random passage of cold clouds (perhaps associated with the BLR?) across the line-of-sight, a more attractive explanation for this is that a substantial ( $> 10^{22}$  cm $^{-2}$ ) amount of photo-ionized material, as discussed in Section 5.1.2, exists along the line-of-sight, but is normally transparent at soft X-ray energies. If the ionizing X-ray flux were unusually low, as in *Ginga* observation 2, the elements

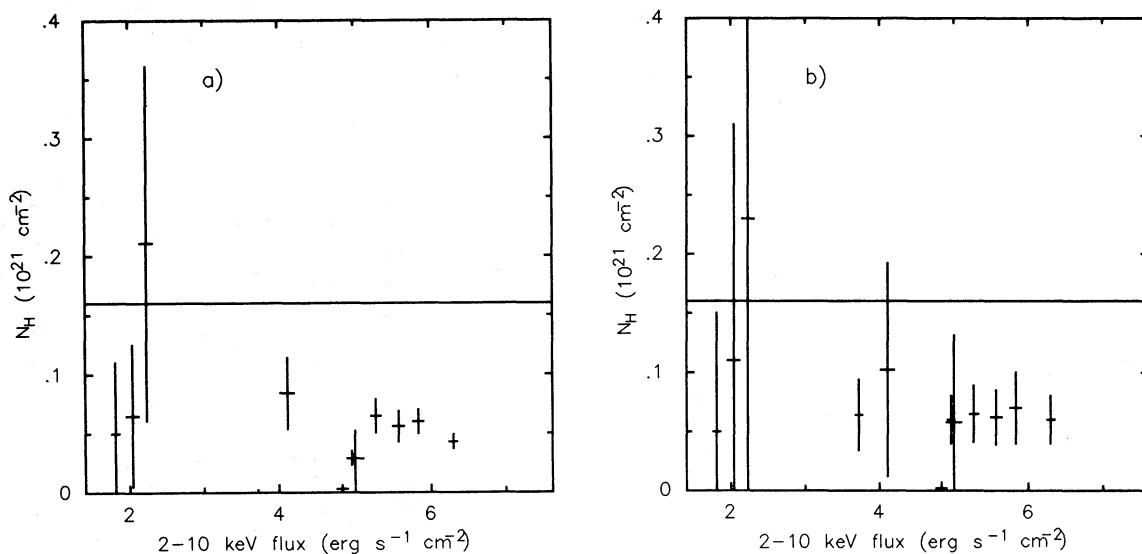


**Figure 7.** Derived  $N_H$  from the power law (left panel) and power law plus disc reflection (right panel) fits to the *EXOSAT* ME and LE data. The solid line represents the absorption by our own Galaxy. An excess of soft photons is inferred in both cases from the fact that the measured columns are significantly lower than that expected if the only absorption is that from our Galaxy.

responsible for absorption at these energies (e.g. O, Si, S, Ar) could recombine. Warm absorber fits [with assumptions as described in Yaqoob, Warwick & Pounds (1989), and photon number index fixed at the average value of 1.83] indicate that a column of  $\sim 4 \times 10^{22} \text{ cm}^{-2}$  with a changing ionization state can describe the variable absorption. For this model, the ionization parameter lies in the range  $U=0.3\text{--}3.3$ , and the implied 0.1–2.0 keV (LE/3 Lx bandpass) flux in the weakest state is a factor of 12 lower than in the brightest case. A variable ‘warm absorber’ can therefore explain the differential variability of the LE and ME fluxes observed by *EXOSAT* (Fig. 1). We would expect such material to leave an imprint at the iron *K*-edge. For the material to be transparent at soft X-ray energies, we expect the edge to occur at 8–9 keV. The *Ginga* data are indeed comparable with such an edge at  $\sim 8$  keV (Table 6). The thermal luminosity of a spherical distribution of such warm material is negligible; however, it may contribute significantly and importantly to the iron *K*-fluorescence, as discussed below.

## 7.2 Origin of the line

From the analysis presented in Section 6.2, we conclude that an accretion disc could be responsible for the majority of the observed iron *K- $\alpha$*  line in NGC 5548. However, the photo-ionized material described above will also contribute to the iron line flux by fluorescence. The suggestion of an iron edge at  $\sim 8$  keV implies a mean ionization state of  $\sim \text{Fe xx}$ . The fluorescent line energy for such ionized iron is around 6.5 eV (Makishima 1986). Such a contribution could resolve the discrepancy mentioned in Section 6.2 between the statistical requirement for a large disc inclination and the large normalization ratio required in such fits. The addition of the ‘blue’ (6.5 keV) wing to the observed line from the warm material would drive the accretion disc reflection fit to a higher inclination, where increased Doppler factors result in a higher mean energy compared to the face-on emission line. According to our modelling (Section 5.1.2), the column density of photo-ionized material required to produce the  $\sim 60$ -eV line for the blue wing is around  $6 \times 10^{22} \text{ cm}^{-2}$ , accounting both for the reduced opacity at  $\sim 6\text{--}7$  keV and the increased fluorescence yield in such a high-ionization state. Such a column is both implied by the iron edge measurements (Table 6) and compatible with the warm column deduced from the low-energy absorption variability described above (Section 7.1). Fitting the reflection model, with  $i=30^\circ$ , together with a line at 6.5 keV provides an excellent description of the observed spectrum. We find a mean value for the equivalent width of 60 eV, in remarkable agreement with the edge measurements. Fits with a line fixed at this mean equivalent width, or with a line flux fixed at  $3 \times 10^{-4} \text{ ph cm}^{-2} \text{ s}^{-1}$  (again, the mean) give  $\chi^2_\nu$  as good as to those for the disc-only fit at  $i=60^\circ$ . The average relative normalization in these fits is now close to 1, and the reflected normalization varies with similar amplitude to the direct continuum. This yields a self-consistent description for the spectrum *and* its variability.

## 7.3 Soft X-ray emission

The composite nature of the X-ray spectrum of NGC 5548 described above has important consequences for previous

models of the soft X-ray emission from the Seyfert nucleus. We find an intrinsic power-law index ( $\Gamma \sim 1.9$ ) systematically steeper than previously reported results (Branduardi-Raymont 1986; Pounds *et al.* 1989). Whilst the inclusion of the reflected component flattens this to  $\sim 1.7$  in the 2–10 keV range, the reflection component is negligible below  $\sim 2$  keV. Fitting a single power-law simultaneously to the *EXOSAT* ME and LE data would then result in an apparent excess of soft photons. This feature, which has been identified in NGC 5548 (e.g. Branduardi-Raymont 1986), does not therefore necessarily represent a separate soft emission component. We have included the disc reflection spectrum in the fit to the *EXOSAT* ME and LE data to check whether strong evidence for a separate soft emission component still exists.

The value of  $N_{\text{H}}$  from our own Galaxy, inferred from 21-cm measurements, is  $1.6 \times 10^{20} \text{ cm}^{-2}$  (Heiles 1975). As found previously, a simple power law yields values for the absorption column substantially lower than this value, indicating an excess of soft photons (Fig. 7a). When the reflection component, with  $i=30^\circ$ , is included a significant soft excess is still apparent (Fig. 7b) in most cases. The evidence for a separate component therefore remains strong, but the total luminosity of the soft X-ray component may have been overestimated in previous analyses. In fact we find that the contribution of any separate soft component to the *EXOSAT* LE flux is not required to be more than 10–20 per cent, if there is no additional absorption, other than the galactic  $N_{\text{H}}$ , below 1 keV. However, the fact that the lowest flux states show little evidence for a soft excess supports our hypothesis that absorption by photo-ionized material is intrinsically important. Our power law plus reflection fits will then underestimate the luminosity of the soft component. The LE/ME lag requirement is in agreement with the implication of a significant contribution below 1 keV from a separate component.

## 7.4 X-ray variability time-scales

The X-ray flux in the hard and soft bands from NGC 5548 varies significantly on time-scales of hours and the flux-doubling/halving time-scale is at most a few days. If the LE variability is simply an extension into the soft band of the ME power-law variability, no useful constraints can be placed on the size of the region producing the soft excess. However, the observed lag ( $\sim$  few hr) between the hard and soft fluxes in NGC 5548 implies that a separate soft component is indeed the major contributor to the observed LE count rate. The size of the soft X-ray emitting material (which might be identified with the inner disc) is therefore similar to that of the hard power-law source.

We can also place a limit on the variability time-scale of the reflected component. Comparing the first and third *Ginga* observations we conclude that the reflected flux must have changed in the  $\sim 6$  months separating these two snapshots. The increase in flux would have otherwise been accompanied by a steepening of the photon index, rather than the flattening actually observed. A similar upper limit ( $\sim 5$  months) is obtained by comparing the third and fourth *Ginga* observations. Unfortunately, due to the poor sampling of the present data, it is impossible to predict the intensity of the reflected continuum in a given observation, as this is a

strong function of the (unobserved) hard X-ray flux history and the precise intrinsic variability time-scale. An upper limit of  $\sim 0.1$  pc can be set on size of the reflecting region by the lack of a positive spectral index correlation between some of the *Ginga* observations, whilst a lower limit of  $\sim 1$  light-day is set by the observed spectral variations. The variation in the normalization of the reflected component is similar to that of the directly viewed power law and suggests that the two regions are of a roughly similar size, although there is clearly no geometry in which the reflector can be smaller than the power-law source, and still subtend a large enough solid angle to produce the features observed here. Furthermore, we consider it unlikely that the reflector is the dusty torus suggested in the Antonucci & Miller scheme since the latter lies between the broad- and narrow-line regions at radii  $\sim 1$  pc. In addition, variability in the reflected component would be significantly 'smoothed out' by light travel time effects in such a scenario contrary to the observed variations. We conclude that the reflecting material lies well within such a torus.

The association of the reflector with the region producing the soft excess leads us to the same conclusion. Whether in the form of blobs or a disc, the rapid variability, correlation with the hard component, of the LE flux observed by *EXOSAT* implies a location close to, and a size similar to the hard source. The presence of the lag rules out the possibility that the cold matter purely reprocesses the hard continuum, contrary to the suggestion of Guilbert & Rees. In fact it seems likely such material is intimately involved in the accretion process, and its thermal emission may represent part of the primary radiation of the active nucleus.

## 8 DISCUSSION

We have shown that both the iron *K*-line emission and apparent spectral index variability observed in NGC 5548 can be explained by a model in which hard X-rays from a power-law source illuminate cold dense material. In order to provide the measured line equivalent width, the material must subtend a large solid angle at the hard X-ray source.

The consequences of the above model for previous views of medium- and low-energy X-ray continua from active galactic nuclei (AGN) are important. First, because the reflected continuum was not resolved with the previous generation of X-ray detectors (on, e.g. *HEAO-1* and *EXOSAT*), the so-called 'canonical' value for X-ray photon spectral indices in the 2–10 keV band,  $\Gamma = 1.7$  (Mushotzky 1984; Turner & Pounds 1989), will have to be modified upwards. Here the intrinsic spectral index ( $\Gamma = 1.8$ – $2.0$ ) of NGC 5548 is not well constrained, as it depends on the precise geometrical model assumed for the reflector. However, we find it to be systematically steeper than previous power-law fits suggest, and steeper than the canonical  $\Gamma = 1.7$ . In a separate analyses of MCG-6-30-15 (Nandra *et al.* 1990), and a composite *Ginga* spectrum (Pounds *et al.* 1990), inclusion of the reflection component resulted in an implied index around 1.9–2.0. These results have significant implications for models of the X-ray emission mechanism in Seyfert-type AGN. In particular underlying indices of order  $\sim 1.9$  revive some electron-positron pair models (Zdziarski *et al.* 1990). Also of interest is a comparison of this result to those of Wilkes & Elvis (1987), who found power-law slopes  $\Gamma \sim 2.0$  for similar radio-quiet AGN in the *Einstein* IPC band (0.5–3.5 keV).

This is consistent with our model, since reflection effects would be negligible in the soft IPC energy band, while the generally more luminous IPC sample may show little absorption.

A second consequence of the steeper intrinsic index implied by our model is that the soft excesses identified by *EXOSAT* and *Einstein* need to be re-assessed. We have shown that a soft emission component is still required by the *EXOSAT* data on NGC 5548, but its significance is reduced. The existence of the ME/LE lag further supports the existence of the soft component in this case, of course. The steeper hard power law implies that the temperature of the soft component (if its origin is thermal) may be somewhat lower than the 0.1–0.2 keV implied by *EXOSAT* spectral fitting to other sources. This has consequences for accretion disc modelling of such excesses. We note in passing that the ultra-soft components found in the *Einstein* IPC spectra of some AGN (Córdova & Kartje 1990) are unlikely to be significantly affected by the assumption of a steeper underlying power law.

The variability time-scales of the various spectral components constrain the size of the reflection region to be less than  $\sim 1.0$  pc, indicating that the matter is close to the central hole. The cold material may be in the form of an accretion disc, or in 'blobs' of the form described by Guilbert & Rees (1988). If the reflector is in the form of a disc, the line profile suggests this is highly inclined. However, the luminosity of the reflected component is then too large to be accounted for by such a disc, unless the hard X-rays are emitted highly anisotropically.

However, in addition to the apparent index variability, positive detections of absorption at 2–3 keV are found for four of the five *Ginga* observations, with variable column density in the range  $\sim 10^{21-22}$  cm $^{-2}$ . Although such column densities may be suggestive of broad-line clouds passing (randomly) through the line-of-sight, the fact that the largest columns (and also the lowest LE band fluxes) are observed in the lowest hard flux states suggests a more interesting possibility. If substantial ionized material with column density  $\sim 5 \times 10^{22}$  cm $^{-2}$  lies along our line-of-sight, the differing amplitudes of variability in the *EXOSAT* ME and LE energy bands can be accounted for by variations in the ionization state of this material. In addition, this photo-ionized gas could also produce a measurable amount of fluorescent iron emission, but at a higher energy compared to the disc (although the two components would be unresolved with the LAC). The inclusion of this second fluorescent line then relaxes the constraints on the disc inclination and normalization, the data then being compatible with a face-on ( $i \sim 30^\circ$ ) disc, without a requirement for significant enhancement of the reflected component. We believe this composite model to be the most plausible description of the X-ray emission in NGC 5548. A physically similar model has already been proposed to explain the X-ray spectrum of MCG-6-30-15 (Nandra, Pounds & Stewart 1990; Nandra *et al.* 1990) and of a composite *Ginga* spectrum (Pounds *et al.* 1990), both of which give similar parameter values to those stated here. This suggests that such features may be common to many Seyfert-type AGN.

Longer or more frequent observations will be necessary to further constrain both the power-law variability time-scale, and that of the reflected flux. Fortunately, these may be available within the lifetime of *Ginga*.

## 9 CONCLUSIONS

To summarize we find the following.

(i) The X-ray spectrum of NGC 5548 is complex, with at least four components. These are, an underlying power law of photon index  $\sim 1.9$ , an iron line of equivalent width  $\sim 130$  eV, a separate soft X-ray emission component and a 'hard tail'. The spectral form is variable, with apparent spectral index changes and variable absorption.

(ii) The bulk of the observed line and the hard tail can be explained by X-ray illumination of cold, optically thick material close to the central source, possibly an accretion disc. The soft emission component may then represent the thermal emission of this material.

(iii) The apparent variability of the spectral index of NGC 5548 is accounted for by differential variability of the underlying power law and the (flatter) Compton reflected continuum radiation.

(iv) The variations in the derived  $N_{\text{H}}$  arise from changes in the ionization state of highly ionized material along the line-of-sight to the central source. These changes also account for the markedly different amplitudes of hard and soft X-ray variability found by EXOSAT.

(v) This material also contributes to the line emission and introduces an absorption edge at  $\sim 8$  keV.

High-resolution X-ray spectroscopy using CCD instruments on the next generation of X-ray satellites (*ASTRO-D*, *SPECTRUM-X*) should be able to establish not only the geometry, column density and ionization state of the matter close to the central engine in AGN, but could also provide information on the dimensions of the emission regions and the ultimate energy source. Further *Ginga* observations, perhaps simultaneous with *ROSAT* may clarify the nature of the soft X-rays, and help quantify the relationship between the hard features and the soft component.

## ACKNOWLEDGMENTS

KN, IMG and GCS acknowledge the SERC for receipt of a Research Studentship, Research Fellowship and Advanced Research Fellowship, respectively.

## REFERENCES

- Antonucci, R. R. J. & Miller, J. S., 1985. *Astrophys. J.*, **297**, 621.  
 Arnaud, K. A., Branduardi-Raymont, G., Culhane, J. L., Fabian, A. C., Hazard, C., McGlynn, T. A., Shafer, R. A., Tennant, A. F. & Ward, M. J., 1985. *Mon. Not. R. astr. Soc.*, **217**, 105.  
 Branduardi-Raymont, G., 1986. *The physics of accretion onto compact objects*, eds Mason, K. O., Watson, M. G. & White, N. E., Springer-Verlag, Berlin.  
 Branduardi-Raymont, G., 1989. *Active Galactic Nuclei*, proc. IAU Symp. No. 124, p. 177, eds Osterbrock, D. E. & Miller, J. S., Reidel, Dordrecht.  
 Chen, K., Halpern, J. P. & Filippenko, A. V., 1989. *Astrophys. J.*, **339**, 742.  
 Córdova, F. A. & Kartje, J. F., 1990. *Proc. 23rd ESLAB symposium on two topics in X-ray astronomy*, eds Hunt, J. & Battrick, B., p. 843.  
 Fabian, A. C., Rees, M. J., Stella, L. & White, N. E., 1989. *Mon. Not. R. astr. Soc.*, **238**, 729.  
 George, I. M. & Fabian, A. C., 1991. *Mon. Not. R. astr. Soc.*, **249**, 352.  
 George, I. M., Nandra, K. & Fabian, A. C., 1990. *Mon. Not. R. astr. Soc.*, **242**, 28p.

- Ghisellini, G., George, I. M., Fabian, A. C. & Done, C., 1991. *Mon. Not. R. astr. Soc.*, **248**, 14.  
 Guilbert, P. W. & Rees, M. J., 1988. *Mon. Not. R. astr. Soc.*, **233**, 475.  
 Halpern, J. P., 1984. *Astrophys. J.*, **281**, 90.  
 Halpern, J. P., 1985. *Astrophys. J.*, **290**, 130.  
 Hayashida, K. *et al.*, 1989. *Publs astr. Soc. Japan*, **41**, 373.  
 Hayes, M. J. C., Culhane, J. L., Blisset, R. J., Barr, P. & Bell Burnell, S. J., 1980. *Mon. Not. R. astr. Soc.*, **193**, 15p.  
 Heiles, C., 1975. *Astr. Astrophys. Suppl.*, **20**, 37.  
 Inoue, H., 1985. *Proc. Japan-US seminar on Galactic and extra-galactic compact X-ray source*, eds Tanaka, Y. & Lewin, W. H. G., ISAS, Tokyo.  
 Kaastra, J. S. & Barr, P., 1989. *Astr. Astrophys.*, **226**, 59.  
 Keel, W. C., 1980. *Astr. J.*, **85**, 198.  
 Krolik, J. H. & Kallman, T. R., 1987. *Astrophys. J.*, **329**, L5.  
 Kunieda, H., Turner, T. J., Hisamitsu, A., Koyama, K., Mushotzky, R. F. & Tsusaka, Y., 1990. *Nature*, **345**, 786.  
 Lawrence, A., Pounds, K. A., Watson, M. G. & Elvis, M., 1985. *Mon. Not. R. astr. Soc.*, **217**, 685.  
 Lightman, A. P. & White, T. R., 1988. *Astrophys. J.*, **335**, 57.  
 Makino, F. & the Astro-C team, 1987. *Astr. Lett. Commun.*, **25**, 223.  
 Makishima, K., 1986. *The physics of accretion onto compact objects*, eds Mason, K. O., Watson, M. G. & White, N. E., Springer-Verlag, Berlin.  
 Malkan, M. A. & Sargent, W. L., 1982. *Astrophys. J.*, **254**, 22.  
 Matsuoka, M., Yamauchi, M., Piro, L. & Murakami, T., 1990. *Astrophys. J.*, in press.  
 Morini, M., Lipani, n. A. & Molteni, D., 1987. *Astrophys. J.*, **317**, 145.  
 Morrison, R. & McCammon, D., 1983. *Astrophys. J.*, **270**, 119.  
 Mushotzky, R. F., 1982. *Astrophys. J.*, **256**, 92.  
 Mushotzky, R. F., 1984. *Adv. Space Res.*, **3**, 157.  
 Mushotzky, R. F., Serlemitsos, P. J., Becker, R. H., Boldt, E. A. & Holt, S. S., 1978. *Astrophys. J.*, **220**, 790.  
 Nandra, K., Pounds, K. A. & Stewart, G. C., 1990. *Mon. Not. R. astr. Soc.*, **242**, 660.  
 Nandra, K., Pounds, K. A., Stewart, G. C., Fabian, A. C. & Rees, M. J., 1989. *Mon. Not. R. astr. Soc.*, **236**, 39p.  
 Nandra, K., Pounds, K. A., Stewart, G. C., George, I. M. & Fabian, A. C., 1990. *Proc. 23rd ESLAB symposium on two topics in X-ray astronomy*, eds Hunt, J. & Battrick, B., p. 1021.  
 Pan, H.-C., Stewart, G. C. & Pounds, K. A., 1990. *Mon. Not. R. astr. Soc.*, **242**, 177.  
 Piro, L., Matsuoka, M. & Yamauchi, M., 1990. *Proc. 23rd ESLAB symposium on two topics in X-ray astronomy*, eds Hunt, J. & Battrick, B., p. 819.  
 Pounds, K. A., Nandra, K., Stewart, G. C. & Leighly, K., 1989. *Mon. Not. R. astr. Soc.*, **240**, 769.  
 Pounds, K. A., Stanger, V. J., Turner, T. J., King, A. R. & Czerny, B., 1986. *Mon. Not. R. astr. Soc.*, **224**, 443.  
 Pounds, K. A., Nandra, K., Stewart, G. C., George, I. M. & Fabian, A. C., 1990. *Nature*, **344**, 132.  
 Shields, G. A., 1978. *Nature*, **272**, 706.  
 Turner, T. J., 1987. *Mon. Not. R. astr. Soc.*, **226**, 9p.  
 Turner, T. J. & Pounds, K. A., 1989. *Mon. Not. R. astr. Soc.*, **240**, 833.  
 Turner, M. J. L. *et al.*, 1990. *Mon. Not. R. astr. Soc.*, **244**, 310.  
 Warwick, R. S., Yaqoob, T., Pounds, K. A., Matsuoka, M. & Yamauchi, M., 1989. *Publs astr. Soc. Japan*, **41**, 721.  
 Wilkes, B. J. & Elvis, M., 1987. *Astrophys. J.*, **323**, 243.  
 Yaqoob, T. & Warwick, R. S., 1991. *Mon. Not. R. astr. Soc.*, **248**, 773.  
 Yaqoob, T., Warwick, R. S. & Pounds, 1989. *Mon. Not. R. astr. Soc.*, **236**, 153.  
 Zdziarski, A. A., Ghisellini, G., George, I. M., Svensson, R., Fabian, A. C. & Done, C., 1990. *Astrophys. J.*, **363**, L1.